Research Square

Preprints are preliminary reports that have not undergone peer review.
They should not be considered conclusive, used to inform clinical practice,
or referenced by the media as validated information.

Multimodal Artificial Intelligence Model Integrating Multiparametric MRI Features and PSA for Differentiating Benign and Malignant Prostate Nodules

Chuangui Li
The First Affiliated Hospital of Hebei North University
Huanying Yin
Hebei North University
Yaying Su
The First Affiliated Hospital of Hebei North University
Xiao Chang
The First Affiliated Hospital of Hebei North University
Huiling Zuo
The First Affiliated Hospital of Hebei North University
Wenjiang Wang
2816508741@qq.com
The First Affiliated Hospital of Hebei North University

Research Article

Keywords: Deep Learning, Radiomics, Prostatic carcinoma, Magnetic Resonance Imaging, PSA

Posted Date: September 28th, 2026

DOI: https://doi.org/10.21203/rs.3.rs-10985839/v1

License: This work is licensed under a Creative Commons Attribution 4.0 International License. Read Full License

Additional Declarations: No competing interests reported.

Abstract

Objective: To develop a multimodal diagnostic model integrating radiomics features, deep learning features derived from prostate multiparametric magnetic resonance imaging (mpMRI), and prostate-specific antigen (PSA) levels, and to investigate its value in differentiating benign and malignant prostate nodules, thereby providing an auxiliary tool for the noninvasive diagnosis of prostate cancer and clinical decision-making.

Methods: A total of 312 patients with prostate nodules confirmed by pathology were retrospectively enrolled and randomly divided into training and test sets at an 8:2 ratio. Radiomics and deep learning features were extracted from T2-weighted imaging (T2WI), diffusion-weighted imaging (DWI), and apparent diffusion coefficient (ADC) maps, and were combined with PSA levels to construct multimodal diagnostic models. Five models were developed, including the ADC model, DWI model, T2WI model, mpMRI model, and mpMRI_PSA model. Five-fold cross-validation was used for model training. Model performance was evaluated in the test set using the area under the receiver operating characteristic (ROC) curve (AUC), accuracy, sensitivity, specificity, positive predictive value, negative predictive value, and F1 score. The DeLong test was used to compare the differences in AUC between the best-performing model and the other models. A *P* value < 0.05 was considered statistically significant.

Results: All five models demonstrated a certain ability to differentiate benign from malignant prostate nodules. The AUCs of the ADC, DWI, T2WI, mpMRI, and mpMRI_PSA models were 0.73, 0.79, 0.84, 0.94, and 0.97, respectively. The diagnostic performance progressively improved with the integration of multiple MRI sequences compared with individual sequences. Further incorporation of PSA resulted in the best diagnostic performance for the mpMRI_PSA model, which outperformed the other models in terms of accuracy, sensitivity, specificity, and F1 score. The DeLong test demonstrated that the differences in AUC between the best-performing mpMRI_PSA model and the ADC, DWI, T2WI, and mpMRI models were all statistically significant ($P < 0.05$).

Conclusion: The multimodal diagnostic model integrating radiomics and deep learning features from prostate mpMRI with PSA levels demonstrated high discriminative performance for differentiating benign and malignant prostate nodules. Its diagnostic performance was superior to that of the single-sequence models and the mpMRI-only model, suggesting that it may serve as a potential auxiliary tool for the noninvasive differential diagnosis of prostate cancer and clinical decision-making.

Introduction

Prostate cancer is one of the most common malignant tumors in men globally and represents a leading cause of cancer-related mortality in the male population[1]. In recent years, driven by population aging, lifestyle changes, and the widespread implementation of prostate-specific antigen (PSA) screening, the incidence of prostate cancer has continuously risen, making it the second most frequent male malignancy worldwide and imposing a heavy burden on public health and social medical resources[2]. Treatment strategies vary substantially across clinical stages, encompassing radical prostatectomy, radiotherapy, androgen deprivation therapy, chemotherapy, and novel targeted therapies[3, 4]. Accurate early diagnosis and timely therapeutic intervention can significantly prolong patient survival, enhance quality of life, and reduce the risk of distant metastasis[5]. Currently, histopathological examination remains the gold standard for prostate cancer diagnosis. However, pathological confirmation typically relies on transrectal or transperineal prostate biopsy, as well as postoperative histopathology. Biopsy is an invasive procedure associated with potential complications such as hemorrhage, infection, and urinary retention[6]. Furthermore, due to limitations in sampling quantity and spatial distribution, biopsy results are susceptible to tumor spatial heterogeneity, potentially leading to missed diagnoses or underestimation of tumor aggressiveness[7]. Although postoperative pathology yields

the most definitive diagnostic results, it is established only after surgical resection, failing to satisfy the demand for preoperative non-invasive evaluation and clinical decision-making. Therefore, developing a non-invasive, accurate, and preoperative computer-aided diagnostic method for differentiating benign from malignant prostate nodules is of paramount clinical importance.

Prostate ultrasonography is widely utilized for initial prostate cancer screening owing to its simplicity, cost-effectiveness, and non-invasive nature[8]. Nevertheless, ultrasound exhibits limited capacity in visualizing internal tissue microstructures and microenvironmental alterations. Consequently, its diagnostic accuracy in differentiating benign from malignant prostate nodules remains relatively low, showing notable performance bottlenecks, particularly in detecting early-stage prostate cancer and atypical lesions[9].

In recent years, with rapid advancements in medical imaging technologies, multiparametric magnetic resonance imaging (mpMRI) has gradually emerged as an essential tool for prostate cancer screening, diagnosis, and risk assessment, and has been incorporated into multiple international clinical guidelines[10]. By integrating anatomical and functional sequences, mpMRI enables multidimensional evaluation of prostate nodules. Key operational sequences include T1-weighted imaging (T1WI), T2-weighted imaging (T2WI), diffusion-weighted imaging (DWI), and apparent diffusion coefficient (ADC) maps. Specifically, T2WI clearly depicts prostate anatomical architecture and lesion morphology[11], whereas DWI and ADC reflect the restriction of tissue water diffusion, thereby indirectly assessing cellular density and tumor aggressiveness[12]. The clinical application of mpMRI has markedly improved the detection rate of clinically significant prostate cancer and demonstrated substantive value in lesion localization, biopsy guidance, tumor staging, risk stratification, and response evaluation during active surveillance[13]. At present, mpMRI has become a cornerstone in the precision diagnosis and treatment paradigm for prostate cancer, significantly driving the development of personalized management.

In addition to imaging modalities, serum PSA remains one of the most widely applied and valuable clinical biomarkers for prostate cancer[14]. Clinical PSA testing primarily evaluates total PSA (tPSA) and free PSA (fPSA), playing a pivotal role in screening, disease monitoring, and prognostic assessment. Elevated PSA levels strongly correlate with an increased risk of prostate cancer occurrence and patient mortality[15]. However, PSA is not a tumor-specific biomarker; its serum concentrations can be confounded by benign prostatic hyperplasia, prostatitis, urinary retention, and recent clinical manipulations, leading to insufficient diagnostic specificity. Consequently, in clinical practice, relying solely on PSA levels for patients with mildly elevated PSA often fails to reliably differentiate malignant from benign nodules. This limitation frequently results in unnecessary biopsies and overtreatment, exacerbating the physical, psychological, and financial burdens on patients. To improve diagnostic accuracy, an increasing number of studies have explored combining imaging findings with serological indicators. For instance, Qi et al.[16] constructed a prostate cancer prediction model by integrating mpMRI radiomic features with clinical parameters. Their findings demonstrated that a combined model fusing radiomic features, PSA density (PSAD), and PI-RADS scores achieved superior diagnostic performance compared to MRI or PSA metrics used in isolation. This indicates that multimodal information fusion can leverage the complementary strengths of imaging phenotypes and clinical biomarkers to elevate the precision of prostate cancer diagnosis.

Concurrently, artificial intelligence (AI) technology has experienced exponential growth in medical imaging, offering promising avenues for the non-invasive precision diagnosis of prostate cancer[17, 18]. Unlike traditional manual reading methods that rely heavily on reader experience, AI can automatically mine and learn latent feature representations from massive medical imaging datasets, uncovering subtle imaging patterns imperceptible to the human eye, thereby enhancing disease detection and classification accuracy. In the realm of prostate cancer

research, deep learning and radiomics have emerged as two of the most representative AI methodologies[19]. Radiomics achieves objective characterization of intratumoral heterogeneity by extracting high-throughput quantitative parameters, including shape, intensity, texture, and high-order features. Conversely, deep learning models, such as convolutional neural networks (CNNs), automatically learn high-dimensional feature representations directly from raw images, overcoming the inherent limitations of manual feature engineering. A wealth of evidence indicates that both approaches effectively enhance prostate cancer detection, Gleason score prediction, and the differentiation between benign and malignant nodules[20].

With the evolving paradigm of multimodal data analysis, researchers increasingly recognize that a single data source is insufficient to fully capture the complex biological behavior of tumors. By integrating heterogeneous information—including MRI imaging features, clinical records, laboratory indicators, and deep learning representations—a more comprehensive characterization of prostate nodules can be established, ultimately improving model performance and generalizability. Prior studies have demonstrated that multimodal AI models consistently outperform single-modality approaches in prostate cancer diagnosis, risk stratification, and outcome prediction[21–24]. Accordingly, this study aims to develop a multimodal AI predictive model that merges radiomics and deep learning features based on prostate MRI images and clinical indicators. We seek to evaluate its application value in differentiating benign from malignant prostate nodules, thereby providing clinicians with an accurate, efficient, and non-invasive diagnostic assistant, as well as novel technical support for early diagnosis and precision management of prostate cancer.

Materials and Methods

General Information

This single-center retrospective study was approved by the Medical Ethics Committee of our hospital (Approval No.: L2026229). The requirement for informed consent was waived due to its retrospective design. Clinical and radiological data of consecutive patients with solitary prostate nodules, who underwent prostate MRI examination and had pathologically confirmed diagnoses between January 2024 and May 2026 at our hospital, were collected. Inclusion criteria: (1) Prostate MRI identified a solitary nodular lesion, pathologically confirmed as benign or malignant via needle biopsy or surgical pathology; (2) The interval between MRI examination and pathological confirmation was within 1 month; (3) MRI image quality met the requirements for lesion segmentation and image analysis; (4) Complete PSA testing results were available within 3 months prior to pathological examination. Exclusion criteria: (1) Prior history of radiotherapy, chemotherapy, endocrine therapy, or other relevant treatments before MRI; (2) Prominent artifacts on MRI images affecting lesion observation and feature extraction; (3) Indistinct nodule boundaries precluding accurate region of interest (ROI) manual delineation; (4) Presence of multiple nodular lesions; (5) Incomplete clinical, radiological, or pathological records. A total of 312 patients with solitary prostate nodules were ultimately enrolled, comprising 126 benign nodules and 186 malignant nodules.

PSA Testing

Fasting venous blood samples (3–5 mL) were collected from all subjects in the morning using non-anticoagulant tubes. After standing at room temperature, the blood was centrifuged at 3000 r/min for 10 min to separate serum for further analysis. Serum PSA levels, including total PSA (tPSA) and free PSA (fPSA), were measured via chemiluminescent immunoassay. All assays were executed on a fully automated immunoassay analyzer (SMART 6500, Serial No.: KSM17650604; Chongqing Cosmida Biological Technology Co., Ltd., Chongqing, China) using the manufacturer's original matching kits, following the manufacturer's instructions strictly. The instrument was calibrated prior to testing, and high- and low-value quality controls were performed; sample testing was conducted

only when quality control results fell within allowable limits. PSA concentration was expressed in ng/mL. The lower limit of detection and linear range of the PSA assays in this study fulfilled clinical requirements. All sample measurements were completed within the same laboratory to minimize inter-batch variability.

Image Acquisition

All patients underwent prostate MRI using a 3.0 T MRI scanner (Philips Healthcare, Best, Netherlands). Patients were placed in the supine position, and image acquisition was performed using a body phased-array coil. The scanning protocol included axial T2WI, DWI, ADC maps. Scanning parameters were configured as follows: T2WI: Repetition time (TR) = 4336 ms, echo time (TE) = 110 ms, slice thickness = 4.5 mm, field of view (FOV) = 244 mm × 244 mm, matrix size = 544 × 432. DWI: TR = 1500 ms, TE = 77 ms, slice thickness = 4.5 mm, FOV = 244 mm × 244 mm, matrix size = 423 × 336. ADC: Automatically generated from the DWI sequence, with a b-value of 1000 s/mm^2 utilized for quantitative analysis.

Data Acquisition and ROI Delineation

T2WI, DWI, and ADC images in DICOM format were exported from the Picture Archiving and Communication System (PACS) for eligible patients. Two radiologists with over 5 years of experience reviewed the images while blinded to the pathological results and reached a consensus. Using 3D Slicer software (version 5.6.2; https://www.slicer.org), manual delineation of the ROI encompassing the prostate nodule was performed on T2WI, DWI, and ADC images for each patient (Fig. 1). Any discrepancies between the two radiologists were resolved through consultation with a third senior radiologist possessing over 10 years of experience.

Radiomics Feature Extraction

Radiomic features were extracted from the T2WI, DWI, and ADC sequences of each patient using the PyRadiomics open-source platform (version 3.0; https://pyradiomics.readthedocs.io/en/latest/). For each sequence (T2WI, DWI, and ADC), a total of 107 radiomic features were extracted per patient, including 14 shape features, 18 first-order statistical features, and 75 texture features. All extracted features subsequently underwent normalization and standardization.

Deep Learning Model Construction and Multimodal Fusion

Each patient was labeled as having a benign or malignant prostate lesion based on histopathological findings. The dataset was randomly partitioned into a training set and a testing set at an 8:2 ratio, yielding 244 cases in the training set and 68 cases in the testing set.

Prior to feature extraction, pixel intensity ranges of raw MRI images across sequences were adjusted to enhance image contrast. Min-max normalization and mean centering were further applied to suppress image noise. For each sequence, the centroid coordinates of the maximum ROI slice were identified and expanded outward to form a 224×224 bounding box, which was used to crop the target region from the raw image. Using the same procedure, the adjacent upper and lower slices were also extracted. These three cropped slices were concatenated to form a 3-channel image input into a ResNet50 CNN.

Within the fully connected layer, deep learning representations and radiomic features were fused for each sequence to construct sequence-specific models (T2WI, DWI, and ADC models). Subsequently, the combined deep learning and radiomic features across all three sequences were merged to build the mpMRI model. Finally, the mpMRI features

were integrated with clinical PSA indicators to establish the comprehensive mpMRI_PSA model. The overall architecture of the multimodal AI pipeline is illustrated in Fig. 2.

During training, a 5-fold cross-validation scheme was employed on the training set. Models were trained for 100 epochs, and the checkpoint achieving the highest validation accuracy was selected. Finally, model performance was evaluated on the independent testing set.

Statistical Analysis

Continuous variables adhering to a normal distribution were presented as mean $\pm$ standard deviation ($\bar{x} \pm s$) and compared between groups using the independent-sample *t*-test. Non-normally distributed continuous variables were expressed as median and interquartile range [*M (Q1, Q3)*] and analyzed using the Mann-Whitney *U* test.

Model predictive performance was comprehensively evaluated using the AUC, accuracy (ACC), sensitivity (SEN), specificity (SPE), positive predictive value (PPV), negative predictive value (NPV), and F1 score. DeLong's test[25] was employed to assess pairwise statistical differences in AUCs among the developed predictive models. Statistical significance was defined as a two-tailed *P*-value *< 0.05*.

Results

PSA Characteristics

The PSA characteristics of the 312 patients with prostate nodules are summarized in Table 1. The Mann-Whitney *U* test demonstrated that both total PSA (tPSA) and free PSA (fPSA) levels were significantly different between the benign and malignant groups (*P < 0.05*).

Table 1
Comparison of serum PSA levels between patients with benign and malignant prostate nodules.

PSA	Benign(ng/mL)	Malignant(ng/mL)	*P*□
tPSA	14.4(6.7, 19.6)	29.5(13.3, 42.8)	0.016
fPSA	1.3(0.8, 2.6)	3.4(1.6, 5.7)	0.036

Loss Curves in Training and Validation Sets

The loss curves of the model on the training and validation sets are illustrated in Fig. 3. A 5-fold cross-validation scheme was employed during model training on the training set. At the onset of training, the loss values were relatively high; however, they stabilized rapidly after approximately 20 iterations. As the number of epochs increased, both the training and validation losses progressively converged, indicating excellent fitting performance without significant overfitting.

Model Performance on the Testing Set

Comparative performance evaluation metrics along with their 95% confidence intervals (CIs) across all developed models are summarized in Table 2. The area under the AUC for the individual sequence models, multi-sequence model, and clinical-radiological multimodal model on the independent testing set were as follows: ADC model: 0.73

(95% CI: 0.62–0.83), DWI model: 0.79 (95% CI: 0.68–0.91), T2WI model: 0.84 (95% CI: 0.74–0.94), mpMRI model: 0.94 (95% CI: 0.87-1.00), mpMRI_PSA model: 0.97 (95% CI: 0.92-1.00).

The ROC curves depicting the diagnostic efficacy of each model are illustrated in Fig. 4. Additional quantitative evaluation metrics—including ACC, SEN, SPE, PPV, NPV, and F1 score—are detailed in Table 3.

Table 2
Predictive performance metrics of different models on the independent testing set

model	AUC (95% CI)	ACC (95% CI)	SEN (95% CI)	SPE (95% CI)	PPV (95% CI)	NPV (95% CI)	F1 score (95% CI)
ADC	0.73(0.62–0.83)	0.66(0.55–0.77)	0.90(0.82–0.97)	0.34(0.25–0.44)	0.65(0.54–0.76)	0.71(0.61–0.82)	0.75(0.65–0.86)
DWI	0.79(0.68–0.91)	0.69(0.56–0.82)	0.87(0.78–0.96)	0.45(0.31–0.59)	0.68(0.55–0.81)	0.72(0.60–0.85)	0.76(0.65–0.88)
T2WI	0.84(0.74–0.94)	0.74(0.61–0.86)	0.85(0.75–0.95)	0.59(0.45–0.72)	0.73(0.61–0.86)	0.74(0.62–0.86)	0.79(0.67–0.90)
mpMRI	0.94(0.87-1.00)	0.84(0.74–0.94)	0.90(0.82–0.98)	0.76(0.64–0.88)	0.83(0.73–0.94)	0.85(0.75–0.95)	0.86(0.77–0.96)
mpMRI_PSA	0.97(0.92-1.00)	0.87(0.78–0.96)	0.95(0.89-1.00)	0.76(0.64–0.88)	0.84(0.74–0.94)	0.92(0.84–0.99)	0.89(0.81–0.98)

To intuitively demonstrate the superiority of the proposed fusion model, confusion matrices for the six models are presented in Fig. 5. The confusion matrices clearly illustrate the classification performance of each model across different diagnostic categories, further confirming the competitive advantage of the fusion model in predictive accuracy.

DeLong's test[25] was performed to evaluate the statistical significance of differences in AUCs between the mpMRI_PSA model and all other candidate models. The pairwise comparison demonstrated that the AUC of the mpMRI_PSA model was significantly higher than those of the individual sequence models and the imaging-only model (all $P < 0.05$; detailed in Table 3).

Table 3
Pairwise comparison of AUCs between the mpMRI_PSA model and other predictive models using DeLong's test.

Model	*P* value
mpMRI_PSA	
ADC	< 0.01
DWI	< 0.01
T2WI	< 0.01
mpMRI	0.04

Discussion

The findings of this study demonstrate that integrating radiomic and deep learning features extracted from T2WI, DWI, and ADC sequences into sequence-specific predictive models yields varying diagnostic performances: the T2WI model outperformed the DWI model, which in turn surpassed the ADC model. Furthermore, combining T2WI, DWI, and ADC sequence features into an integrated mpMRI model yielded superior AUC values compared to any single-sequence model, demonstrating enhanced diagnostic efficacy. Crucially, the multimodal mpMRI_PSA model—which incorporates clinical PSA indicators—achieved the highest ACC, SEN, SPE, PPV, NPV, and F1 score, underscoring its superior predictive robustness and generalizability in differentiating benign from malignant prostate nodules.

In clinical practice, radiologists typically rely on T2WI sequences to identify nodule localization (whether within the peripheral zone or transition zone) and morphology, providing pivotal diagnostic cues for determining malignancy risk[26]. Hyperintensity on DWI corresponds to increased cellular density, whereas corresponding hypointensity on ADC maps signifies restricted water molecule diffusion—a pathognomonic micro-pathophysiological feature of malignant tumors. This rationale motivated our selection of these three core sequences. Conversely, T1WI was excluded because it provides minimal contrast resolution for soft-tissue lesions and intraprostatic nodules, making visual identification challenging. Nevertheless, the combination of DWI hyperintensity and ADC hypointensity is not entirely pathognomonic for malignancy. Numerous non-malignant conditions exhibit confounding diffusion restriction, creating diagnostic "false positives". For instance, acute or active chronic prostatitis causes elevated DWI signals and decreased ADC values due to inflammatory cell infiltration and stromal edema, overlapping significantly with prostate cancer features. Similarly, benign prostatic hyperplasia nodules—particularly stroma-rich subtypes—exhibit high cellular packing that restricts diffusion to a degree. Furthermore, post-biopsy hemorrhage accompanied by localized inflammatory reactions and hemosiderin deposition can obscure true DWI signal interpretation. These factors introduce substantial ambiguity when relying solely on DWI/ADC thresholding; even when combined with T2WI morphological findings, diagnostic pitfalls remain difficult to avoid entirely. Simultaneously, while serum PSA is the most widely utilized biomarker for prostate cancer screening, its utility for distinguishing benign from malignant nodules remains constrained. Although PSA exhibits high organ specificity (secreted by prostate epithelial cells), its tumor specificity is suboptimal. Elevated PSA levels frequently stem from non-malignant conditions, primarily prostatic hyperplasia nodules—where expanded glandular volume elevates total PSA secretion—as well as prostatitis and clinical manipulations. Therefore, by employing AI to fuse T2WI, DWI, ADC, and serum PSA, our study aims to mitigate single-modality limitations and optimize non-invasive diagnostic precision.

In recent years, AI-driven differentiation of prostate nodules has evolved rapidly, with numerous studies demonstrating the utility of radiomics, deep learning, and machine learning models in prostate cancer detection. Xu et al.[27] developed deep learning models to analyze mpMRI for automated prostate cancer diagnosis, highlighting the capability of deep learning in extracting latent imaging representations. However, their study relied exclusively on automated deep learning features without incorporating clinical biomarkers or quantitative radiomic parameters. In contrast, our pipeline fuses radiomics, deep learning, and PSA indicators, leveraging the synergistic strengths of heterogeneous data to achieve more comprehensive lesion characterization. Lu et al. [28] constructed a biparametric MRI radiomics model to differentiate prostatic hyperplasia nodules from prostate cancer and observed that performance improved upon adding clinical PSA metrics, reinforcing the value of fusing imaging with clinical records. Nevertheless, hand-crafted radiomic features have inherent limitations in capturing high-order nonlinear abstractions. By integrating ResNet50 deep learning representations with radiomics across T2WI, DWI, and ADC sequences, our approach captures richer intratumoral heterogeneity. Similarly, Zhou et al.[29] built machine learning models based on mpMRI radiomics for preoperative nodule differentiation, confirming the feasibility of quantitative imaging analysis. However, traditional machine learning relies heavily on feature engineering and selection heuristics. Deep learning automatically learns complex high-dimensional spatial patterns, complementing handcrafted radiomic features and

clinical PSA biology to bolster model stability and generalizability. Collectively, multi-source data fusion represents a pivotal paradigm shift in prostate AI diagnostics. The superior diagnostic performance achieved by our multimodal model confirms that deeply integrating multi-sequence imaging with clinical biomarkers provides a more reliable non-invasive decision-support system.

This study sought to establish a multimodal AI prediction model via quantitative analysis of prostate MRI images and serum PSA levels for precise nodule differentiation. In clinical settings, prostate cancer diagnosis necessitates synthesizing imaging findings, laboratory metrics, and histopathology; single-modality assessments rarely capture the full biological continuum[30]. To address this, we employed ResNet50 as our deep learning backbone and applied transfer learning to enhance feature extraction capabilities. During multimodal fusion, feature vectors from disparate sources were concatenated at the fully connected layer to enable joint modeling. Among single-sequence models, T2WI performed best. This superior efficacy likely stems from its high spatial resolution, which clearly delineates anatomical boundaries, capsule integrity, and subtle tissue contrast. Conversely, ADC maps focus primarily on functional diffusion restriction and lack fine anatomical detail, potentially limiting single-sequence performance. Notably, Le et al.[31] reported that an ADC single-sequence CNN model outperformed its T2WI counterpart, contrasting with our findings. This discrepancy may be attributed to differences in data preprocessing: Le et al. applied extensive data augmentation—such as random translations, rotations, and flipping—which, while increasing sample volume, may introduce non-rigid deformations that alter fine anatomical features and spatial relationships. In contrast, we omitted synthetic spatial transformations to preserve authentic anatomical architecture. Furthermore, our findings align with Bertelli et al.[32], who emphasized the pivotal role of T2WI due to its superior spatial and contrast resolution in prostate lesion identification. Crucially, combining T2WI, DWI, and ADC yielded significant performance gains over any single sequence, confirming the complementary nature of structural and functional sequences. Adding PSA to the mpMRI feature space achieved the overall highest diagnostic efficacy (*AUC = 0.97*), validating the premise that combining radiological phenotypes with systemic clinical biomarkers significantly sharpens diagnostic accuracy. Furthermore, co-extracting handcrafted radiomic features and deep learning representations fuses domain-specific interpretability with automated feature learning capabilities—a multi-feature fusion strategy whose efficacy has been validated across broader medical imaging domains[33].

Several limitations of this study warrant consideration. First, lesion ROI delineation was performed manually. Although standardized guidelines were strictly followed, manual segmentation remains susceptible to inter-observer variability and operator experience; future iterations should incorporate automated or semi-automated segmentation algorithms to enhance reproducibility. Second, this was a single-center retrospective study with a relatively modest sample size and no external validation cohort; the generalizability of our model requires rigorous verification across multi-center, large-scale prospective cohorts. Third, our study cohort was restricted to patients with solitary prostate nodules; model performance in multi-focal disease warrants dedicated investigation. Finally, our feature space was limited to multiparametric MRI and serum PSA. Future research should explore integrating additional advanced diagnostic modalities, such as PSMA-PET/CT imaging and molecular biomarkers, to further refine diagnostic accuracy and clinical translation value.

Conclusion

In this study, a multimodal AI diagnostic framework was constructed by integrating multiparametric MRI features, quantitative radiomics, deep learning representations, and serum PSA levels. The empirical results demonstrate that fusing mpMRI multimodal imaging features with clinical PSA significantly improves the differential diagnosis of benign and malignant prostate nodules, outperforming both single-sequence models and the imaging-only mpMRI

model. The proposed model exhibits outstanding diagnostic accuracy and robustness, offering a non-invasive, efficient decision-support tool for early prostate cancer detection, risk stratification, and personalized clinical management.

Declarations

Author Contribution

C.L. and W.W. conceived and designed the study. C.L., H.Y., Y.S., X.C., and H.Z. contributed to patient enrollment, data collection, and clinical information acquisition. W.W. performed image processing, radiomics and deep learning feature extraction, model development, statistical analysis, and manuscript drafting. C.L. and W.W. interpreted the results and critically revised the manuscript. All authors reviewed and approved the final manuscript.

References

1. Bray F, Laversanne M, Sung H, et al. Global cancer statistics 2022: GLOBOCAN estimates of incidence and mortality worldwide for 36 cancers in 185 countries[J]. CA: A Cancer Journal for Clinicians, 2024, 74(3): 229–263.
2. Kratzer T B, Mazzitelli N, Star J, et al. Prostate cancer statistics, 2025[J]. CA: A Cancer Journal for Clinicians, 2025, 75(6): 485–497.
3. Li X, Han Z, Ai J. Synergistic targeting strategies for prostate cancer[J]. Nature Reviews Urology, 2025, 22(10): 645–671.
4. Rai V. Immune Checkpoint Inhibitor Therapy for Prostate Cancer: Present and Future Prospectives[J]. Biomolecules, 2025, 15(6): 751.
5. Hugosson J, Godtman R A, Wallstrom J, et al. Results after Four Years of Screening for Prostate Cancer with PSA and MRI[J]. New England Journal of Medicine, 2024, 391(12): 1083–1095.
6. Loeb S, Vellekoop A, Ahmed H U, et al. Systematic Review of Complications of Prostate Biopsy[J]. European Urology, 2013, 64(6): 876–892.
7. Ruijter E, Van Leenders G, Miller G, et al. Errors in histological grading by prostatic needle biopsy specimens: frequency and predisposing factors[J]. The Journal of Pathology, 2000, 192(2): 229–233.
8. Tang Y, Li X, Jiang Q, et al. Diagnostic accuracy of multiparametric ultrasound in the diagnosis of prostate cancer: systematic review and meta-analysis[J]. Insights into Imaging, 2023, 14(1): 203.
9. Ditonno F, Franco A, Manfredi C, et al. Novel non-MRI imaging techniques for primary diagnosis of prostate cancer: micro-ultrasound, contrast-enhanced ultrasound, elastography, multiparametric ultrasound, and PSMA PET/CT[J]. Prostate Cancer and Prostatic Diseases, 2024, 27(1): 29–36.
10. Hamm C A, Baumgärtner G L, Biessmann F, et al. Interactive explainable deep learning model informs prostate cancer diagnosis at MRI[J]. Radiology, 2023, 307(4): e222276.
11. Kim D H, Choi M H, Lee Y J, et al. Deep learning-accelerated T2WI of the prostate for transition zone lesion evaluation and extraprostatic extension assessment[J]. Scientific Reports, 2024, 14(1): 29249.
12. Zhang K, Zhang C, Chen Z, et al. Objective value of the apparent diffusion coefficient (ADC) map fromUltrahigh b-value diffusion-weighted imaging (DWI) in 3T MRI could be aNon-invasive specific biomarker for prostate cancer[J]. Current Medical Imaging Reviews, 2023, 20: e180723218855.

13. Thompson J E, Van Leeuwen P J, Moses D, et al. The Diagnostic Performance of Multiparametric Magnetic Resonance Imaging to Detect Significant Prostate Cancer[J]. Journal of Urology, 2016, 195(5): 1428–1435.
14. Stenman U H, Leinonen J, Zhang W M. Standardization of PSA determinations[J]. Scandinavian Journal of Clinical and Laboratory Investigation, 1995, 55(sup221): 45–51.
15. Jehle D V K, Nguyen N, Garza M A, et al. PSA Levels and Mortality in Prostate Cancer Patients[J]. Clinical Genitourinary Cancer, 2024, 22(5): 102162.
16. Qi Y, Zhang S, Wei J, et al. Multiparametric MRI-Based Radiomics for Prostate Cancer Screening With PSA in 4–10 ng/mL to Reduce Unnecessary Biopsies[J]. Journal of Magnetic Resonance Imaging, 2020, 51(6): 1890–1899.
17. Arigbede O, Amusa T, Buxbaum S G. Exploring the Use of Artificial Intelligence and Robotics in Prostate Cancer Management[J]. Cureus, 2023.
18. Nayan M, Salari K, Bozzo A, et al. A machine learning approach to predict progression on active surveillance for prostate cancer[J]. Urologic Oncology: Seminars and Original Investigations, 2022, 40(4): 161.e1-161.e7.
19. Yang X, Fan X, Lin S, et al. Assessment of Lymphovascular Invasion in Breast Cancer Using a Combined MRI Morphological Features, Radiomics, and Deep Learning Approach Based on Dynamic Contrast-Enhanced MRI[J]. Journal of magnetic resonance imaging: JMRI, 2023.
20. Vakili S, Beheshti I, Barzegar Behrooz A, et al. Transforming Prostate Cancer Care: Innovations in Diagnosis, Treatment, and Future Directions[J]. International Journal of Molecular Sciences, 2025, 26(11): 5386.
21. Gallivanone F, Bertoli G, Porro D. Radiogenomics, Breast Cancer Diagnosis and Characterization: Current Status and Future Directions[J]. Methods and Protocols, 2022, 5(5): 78.
22. LeCun Y, Bengio Y, Hinton G. Deep learning[J]. Nature, 2015, 521(7553): 436–444.
23. Lei Y M, Yin M, Yu M H, et al. Artificial Intelligence in Medical Imaging of the Breast[J]. Frontiers in Oncology, 2021, 11: 600557.
24. Jiang Y, Edwards A V, Newstead G M. Artificial Intelligence Applied to Breast MRI for Improved Diagnosis[J]. Radiology, 2021, 298(1): 38–46.
25. DeLong E R, DeLong D M, Clarke-Pearson D L. Comparing the Areas under Two or More Correlated Receiver Operating Characteristic Curves: A Nonparametric Approach[J]. Biometrics, 1988, 44(3): 837–845.
26. Purysko A S, Rosenkrantz A B, Barentsz J O, et al. PI-RADS version 2: a pictorial update[J]. RadioGraphics, 2016, 36(5): 1354–1372.
27. Xu Y, Wang R, Fang Z, et al. Feasibility study of AI-assisted multi-parameter MRI diagnosis of prostate cancer[J]. Scientific Reports, 2025, 15(1): 10530.
28. Lu Y, Yuan R, Su Y, et al. Biparametric MRI-based radiomics for noninvastive discrimination of benign prostatic hyperplasia nodules (BPH) and prostate cancer nodules: a bio-centric retrospective cohort study[J]. Scientific Reports, 2025, 15(1): 654–665.
29. Zhou W, Liu Z, Zhang J, et al. Interpretable multiparametric MRI radiomics-based machine learning model for preoperative differentiation between benign and malignant prostate masses: a diagnostic, multicenter study[J]. Frontiers in Oncology, 2025, 15: 1541618.
30. Brondani Torri G, Antune Pereira P, Piovesan Wiethan C, et al. Comparison of Multiparametric MRI and the Combination of PSMA Plus MRI for the Intraprostatic Diagnosis of Prostate Cancer: A Systematic Review and Meta-Analysis[J]. Clinical Nuclear Medicine, 2024, 49(8): e375-e382.
31. Le M H, Chen J, Wang L, et al. Automated diagnosis of prostate cancer in multi-parametric MRI based on multimodal convolutional neural networks[J]. Physics in Medicine & Biology, 2017, 62(16): 6497–6514.

32. Bertelli E. Machine and deep learning prediction of prostate cancer aggressiveness using multiparametric MRI[J]. 0–14.
33. Wang W, Li J, Wang Z, et al. Study on the classification of benign and malignant breast lesions using a multi-sequence breast MRI fusion radiomics and deep learning model[J]. European Journal of Radiology Open, 2024, 13(1): 100607.

Figures

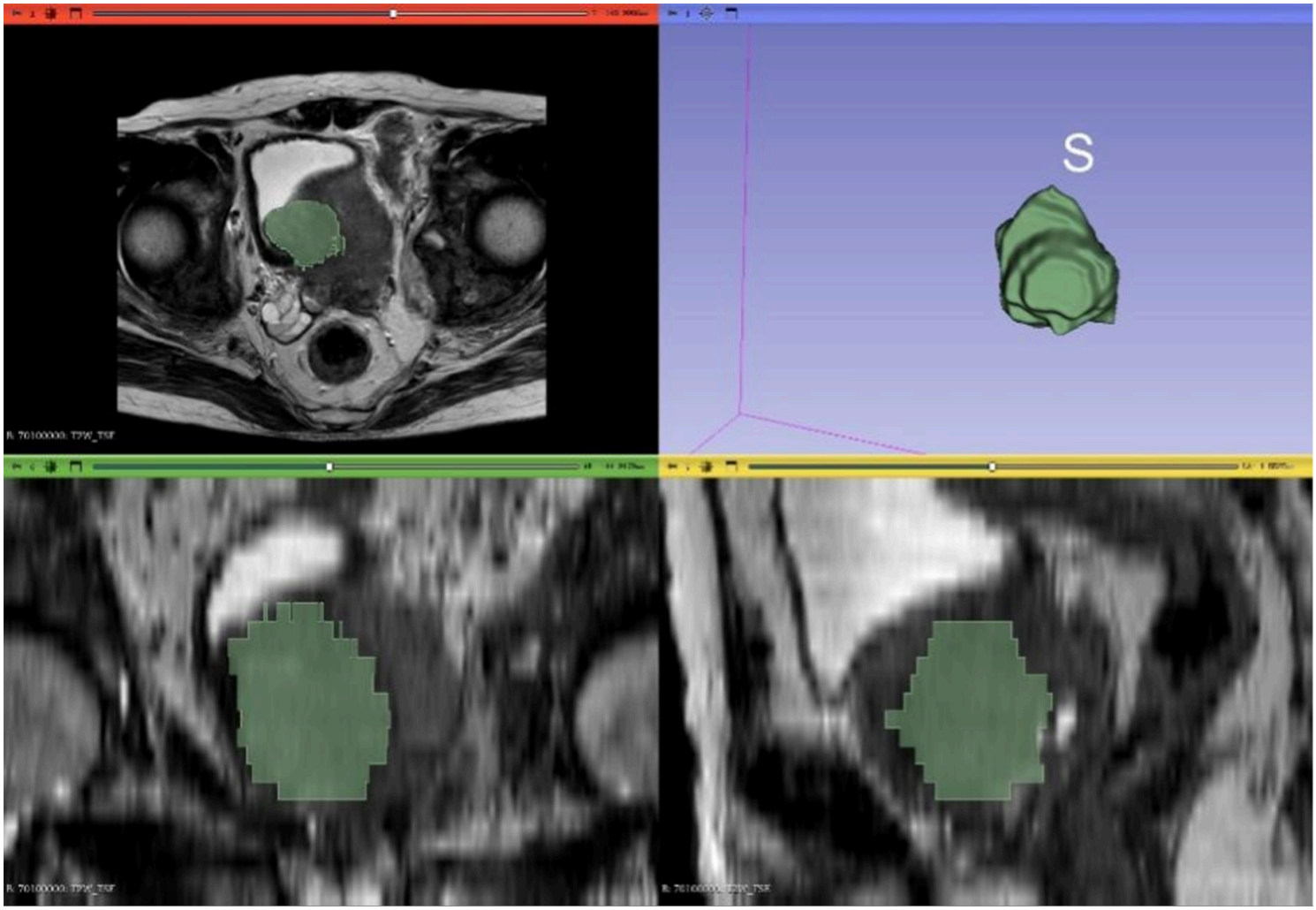


Figure 1

Representative ROI manual delineation of a prostate nodule across MRI sequences.

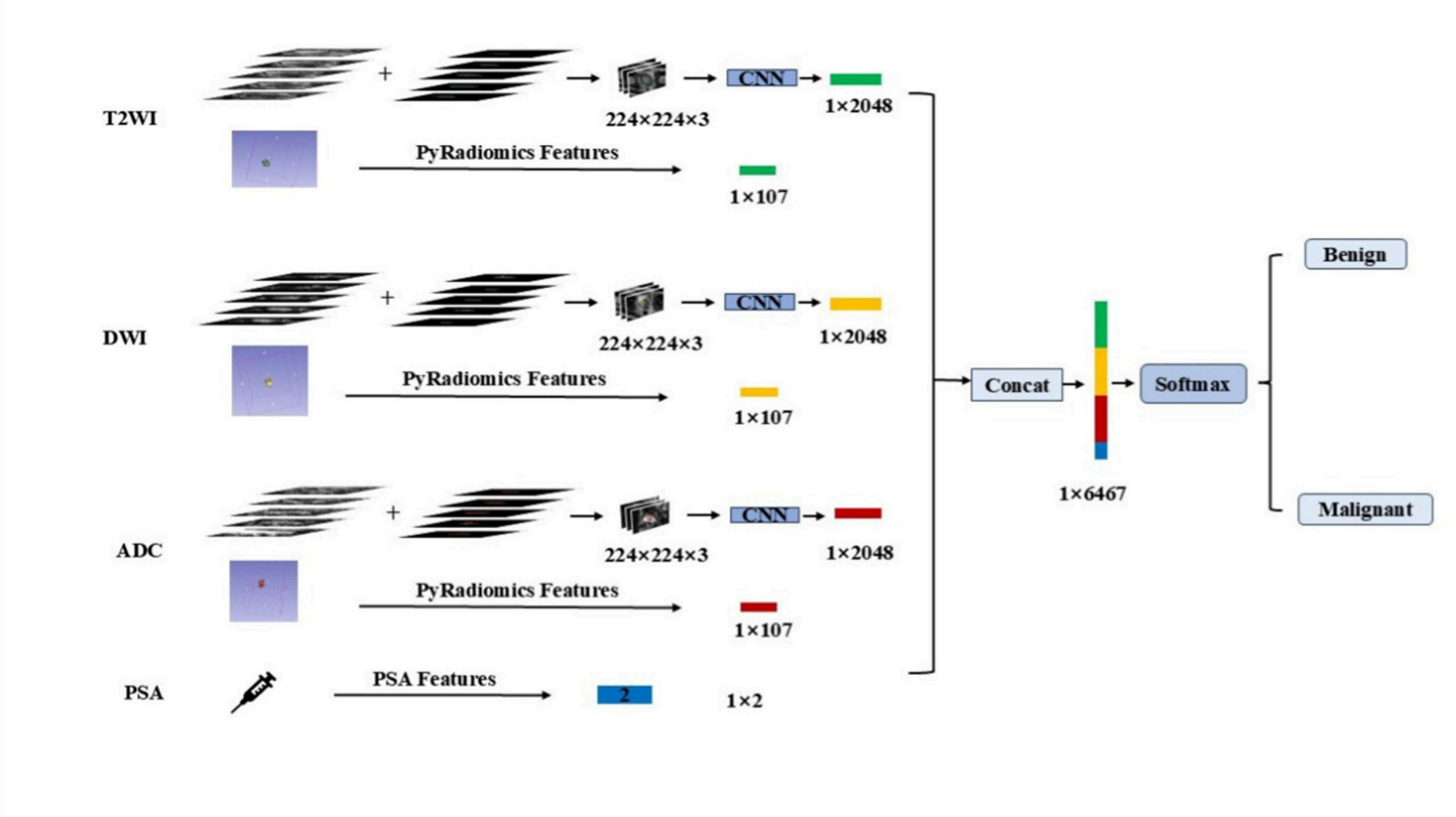


Figure 2

Schematic diagram of the proposed multimodal fusion network architecture. T2WI, T2-weighted imaging; DWI, diffusion-weighted imaging; ADC, apparent diffusion coefficient; PSA, prostate-specific antigen; CNN, convolutional neural network; Concat, feature concatenation; Softmax, softmax activation function; Benign, benign prostate nodule; Malignant, malignant prostate nodule.

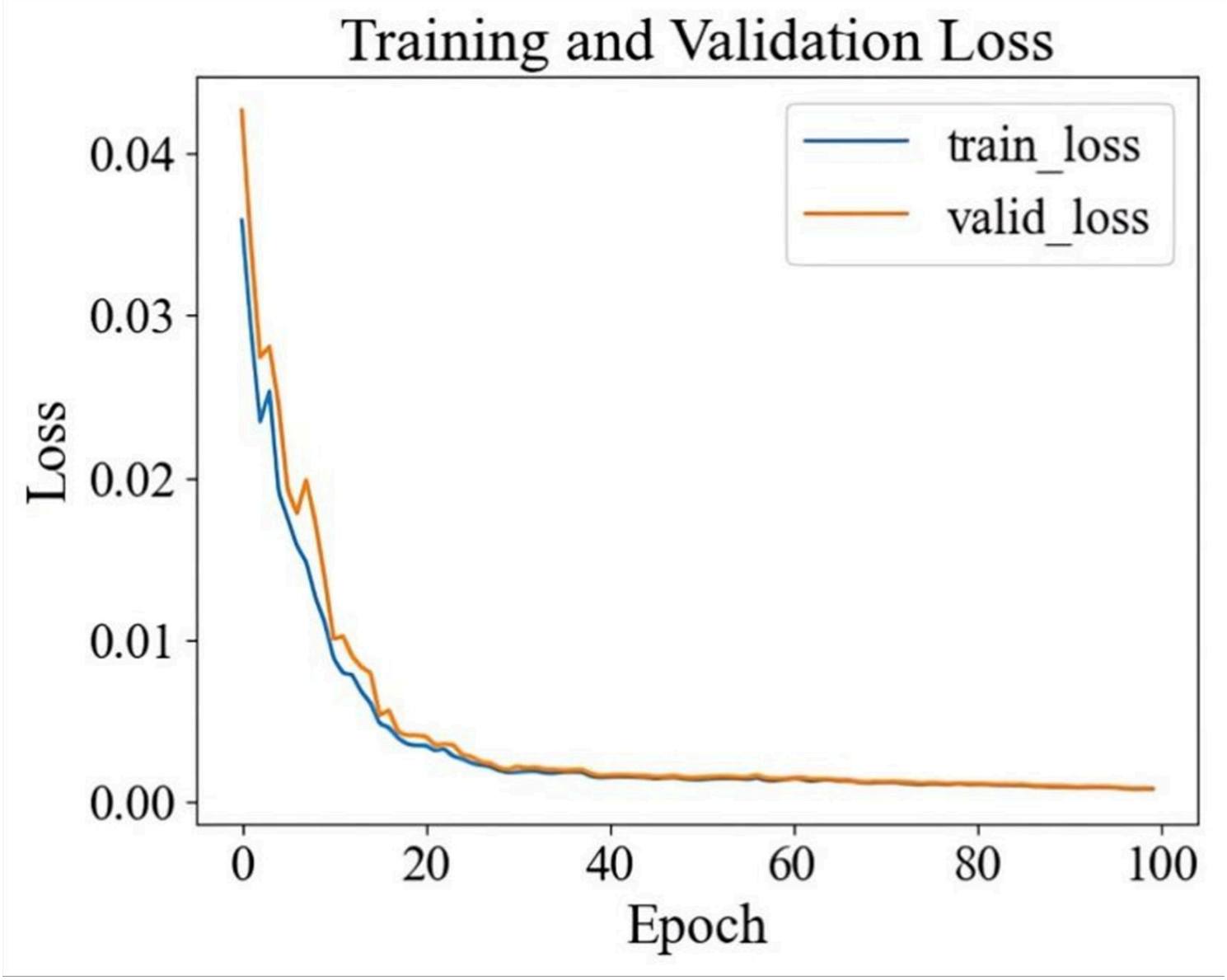


Figure 3

Training and validation loss curves of the proposed multimodal fusion model. A 5-fold cross-validation scheme was implemented during model training. The blue curve denotes the training loss averaged across the five folds, while the yellow curve represents the corresponding validation loss. Both loss trajectories stabilize and converge after approximately 20 epochs, indicating robust convergence without significant overfitting.

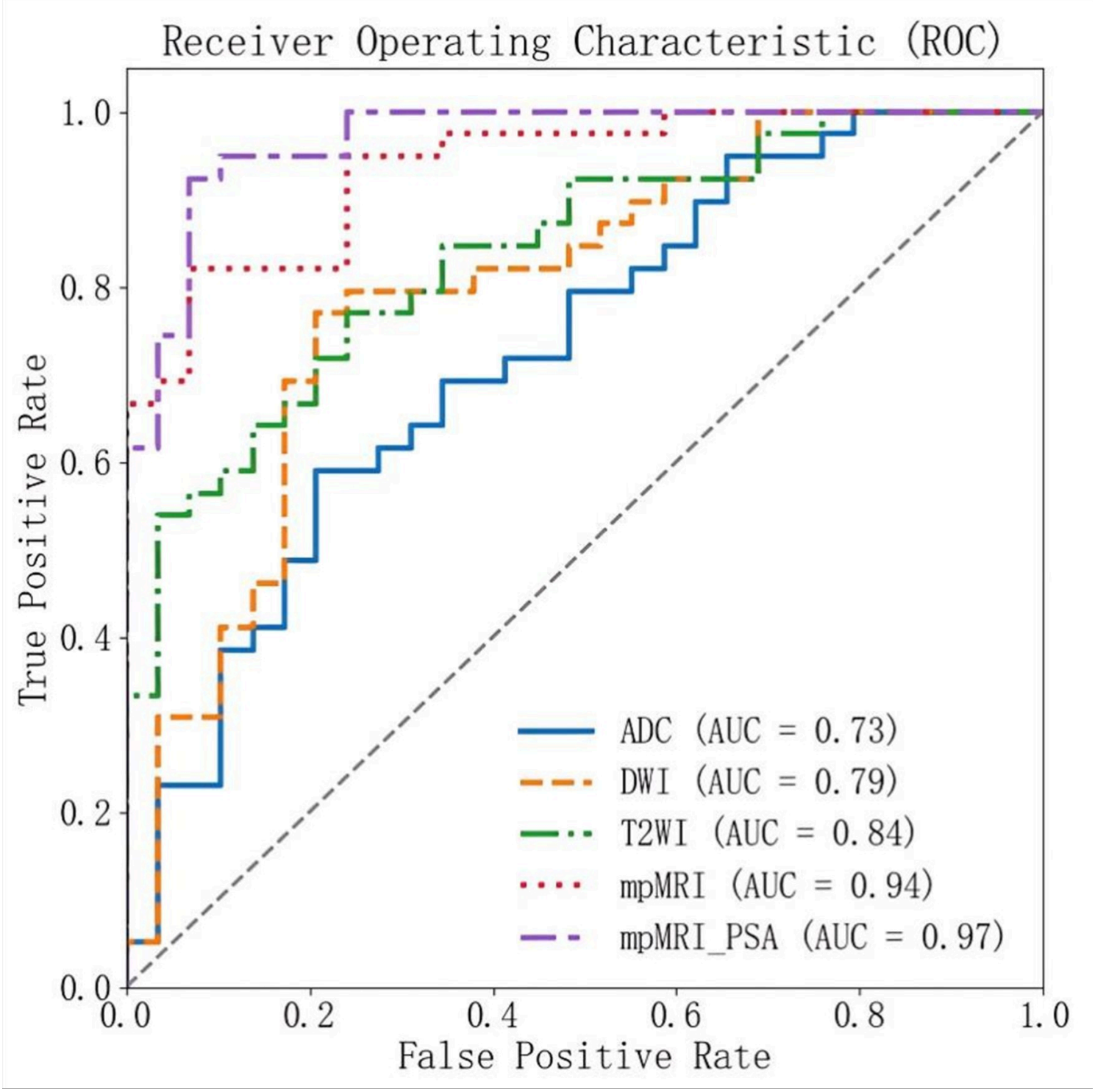


Figure 4

ROC curves of different predictive models on the independent testing set

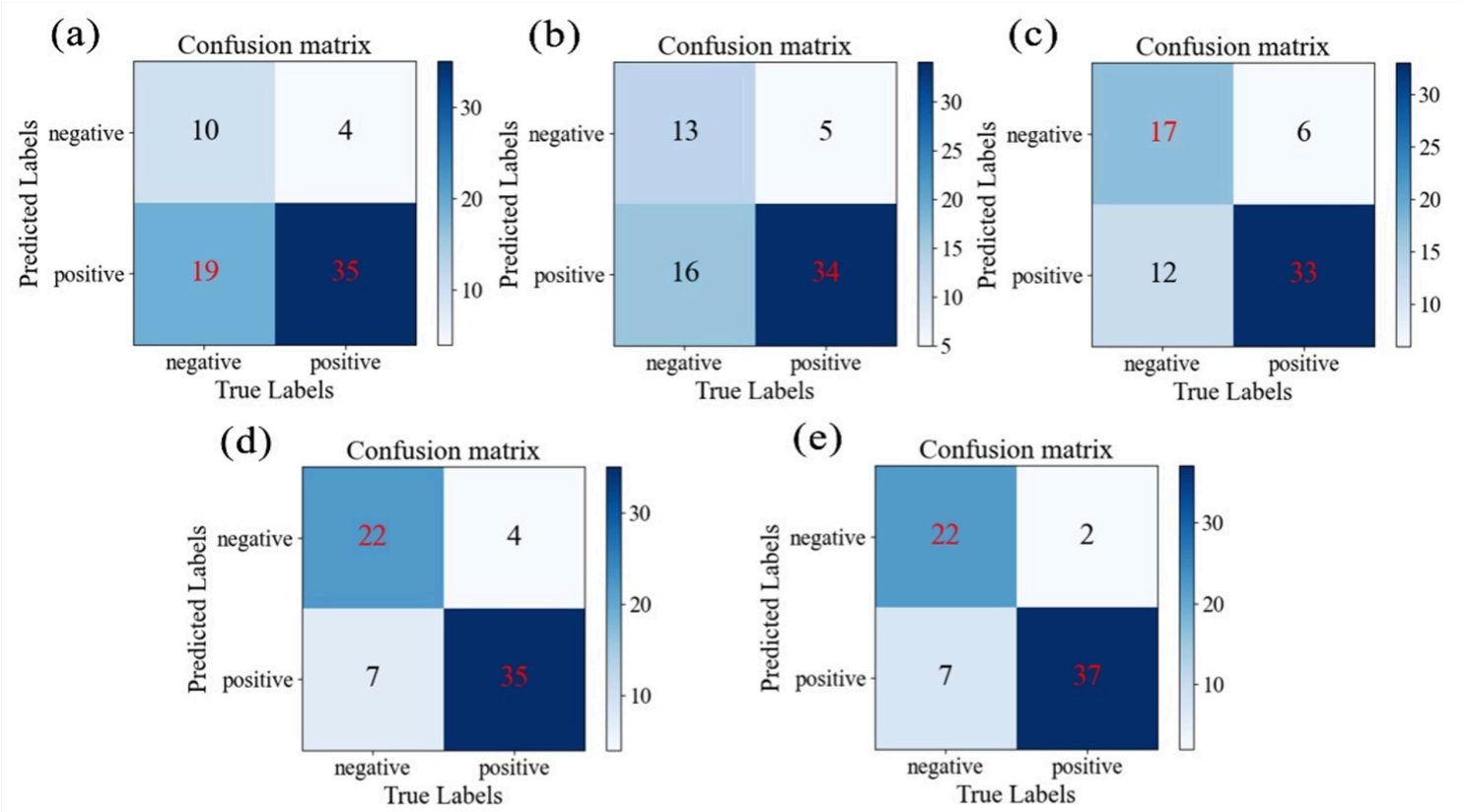


Figure 5

Confusion matrices of different predictive models on the independent testing set. (a) Confusion matrix of the ADC model; (b) Confusion matrix of the DWI model; (c) Confusion matrix of the T2WI model; (d) Confusion matrix of the mpMRI model; (e) Confusion matrix of the multimodal mpMRI_PSA model.